Desalination and Water Treatment
www.deswater.com

doi: 10.1080/19443994.2014.906324

54 (2015) 3134–3145
June

Taylor & Francis
Taylor & Francis Group

Solar, visible and UV light photocatalytic activity of $CoWO_4$ for the decolourization of methyl orange

Kandasamy Jothivenkatachalam[a,*], Saravanan Prabhu[a], Arjunan Nithya[a], Singaravelu Chandra Mohan[a], Kulandaivel Jeganathan[b]

[a]*Department of Chemistry, Anna University, BIT Campus, Tiruchirappalli 620 024, Tamil Nadu, India, Tel. +91 9443215423; email: jothivenkat@yahoo.com (K. Jothivenkatachalam), Tel. +91 9942549466; email: s.sprabhuk@gmail.com (S. Prabhu), Tel. +91 9486292229; email: nithiarjunan@yahoo.co.in (A. Nithya), Tel. +91 9944762077; email: chemcm@gmail.com (S. Chandra Mohan)*

[b]*Centre for Nanoscience and Nanotechnology, School of Physics, Bharathidasan University, Tiruchirappalli 620 024, Tamil Nadu, India, Fax: +91 431 2497 045, 2407 020; email: kjeganathan@yahoo.com (K. Jeganathan)*

Received 5 October 2013; Accepted 12 March 2014

ABSTRACT

The photocatalyst $CoWO_4$ was synthesized by co-precipitation method with slight modification and well characterized by FT-IR, UV–vis diffuse reflectance spectra, X-ray diffraction, AFM and field emission scanning electron microscope techniques. The elemental composition present in the photocatalyst was confirmed by recording EDX spectrum. The photocatalytic activity of $CoWO_4$ for the decolourization of methyl orange (MO) was investigated under solar, visible and Ultra-Violet (UV) light irradiation. The remarkable photocatalytic decolourization of MO was achieved under solar and visible light irradiation than that of TiO_2. The high surface area of 55.0527 m/g enhances the adsorption of anionic dye MO on the surface of the positively charged catalyst at pH 3 thus increases the photocatalytic activity. Under UV light irradiation, photocatalytic activity increases which may be due to high energy of photons. The essential parameters such as amount of catalyst, dye concentration and initial pH influence the photocatalytic efficiency of $CoWO_4$. The first order rate constant for the decolourization reaction was derived using Langmuir–Hinshelwood kinetic model.

Keywords: Photocatalysis; Methyl orange (MO); UV-light; Solar light; Visible light; $CoWO_4$; Decolourization

1. Introduction

The industrial process such as textile manufacturing involves a sequence of steps which produces large amount of waste water. Usually this effluent has low BOD and high COD content which is caused by the intense colour of the dyes, contaminant like surfactant, sizing agent, high salinity and abnormal pH [1]. In every year 0.7 millions of synthetic dyes are manufactured [2] and mainly used in textile, leather goods, industrial painting, food, plastics, cosmetics and consumer electronic sectors. The effluent from the above industries with high toxicity causes water pollution. Several techniques were used for the treatment of this effluent. These are adsorption on activated carbon, ultra filtration, reverse osmosis, biodegradation, chlorination and ozonation which are relatively inefficient for almost all dyes and with high operation cost. In

---

*Corresponding author.

recent years, researchers have mainly focused on the heterogeneous photocatalysis. Photocatalysis is a promising technique to decontaminate the environment and to provide clean and recyclable hydrogen energy by water splitting. Using this process, solar energy can be utilized to degrade the harmful organic and inorganic materials present in air and aqueous phase [3–6]. This process has gained additional importance due to its non-toxicity, works at ambient temperature and low cost [7]. Many attempts have been made to degrade mono-azo dyes particularly Acid Orange7 and methyl orange (MO). These dyes are extensively used in textiles, foodstuffs, pulp, paper and leather industry. The effluent of these dyes and its by-products can cause environmental problems like water pollution and toxicity.

TiO_2 is the best candidate and widely used photocatalytic material. Since fraction of solar light (4%) can be utilized due to its wide band gap of about 3.2 eV, it cannot be activated under visible light [8,9]. Nitrogen-doped TiO_2 is recently reported as a visible light photocatalyst [8,10,11]. The quantum efficiency of nitrogen-doped TiO_2 is lower under visible light irradiation [11]. In contrast, a class of "multi metal component" oxide semiconductors like divalent metal tungstates ($M^{II}WO_4$) has gained additional importance. Even though they have thermal and chemical stability, very few literature reports are available for $M^{II}WO_4$ used as photocatalysts [12,13]. Y. Zhu group was reported the degradation of Rhodamine B by $ZnWO_4$ [14,15]. The photocatalytic activity of $ZnWO_4$ has been enhanced by doping with fluorine [16]. Fu et al. [12] have evaluated the photocatalytic activity of Bi_2WO_6 and $PbWO_4$ under visible light irradiation. Montini et al. [17] have discussed the photocatalytic performance of transition metal tungstates under visible light irradiation for the degradation of methylene blue and MO. The high photocatalytic activity was achieved by $ZnWO_4$. However, $CoWO_4$ have inability to degrade the MO.

In this paper, an attempt is made to enhance the photocatalytic activity of $CoWO_4$ by changing synthesis method and conditions. To synthesis the metal tungstate, several methods are available which includes conventional solid-state reactions, co-precipitation and hydrothermal methods. Among the several methods, we adopted co-precipitation method with slight modification. To further understand the photocatalytic activity of $CoWO_4$, we have investigated the effect of various light irradiations such as solar, visible and UV. The photocatalytic activity was compared with commercially available TiO_2. To the best of our knowledge, this is the first evidence that $CoWO_4$ can be used as an efficient photocatalyst for the decolourization of MO under solar, visible as well as UV light irradiation.

2. Experimental set-up

2.1. Materials

All analytical grade reagents of Cobalt(II)acetatetetrahydrate, Sodium tungstate dihydrate, MO, TiO_2, NaOH and H_2SO_4 were used as such without further purification. Deionized and double distilled water was used throughout this work. The pH of the solutions was monitored using ELICO LI120 pH meter.

2.2. Preparation of photocatalyst

The photocatalyst $CoWO_4$ was prepared by co-precipitation method [18,19] with slight modification as follows. Aqueous solutions of Cobalt acetate tetrahydrate and sodium tungstate dihydrate were prepared separately to obtain a clear solution. Aqueous solutions were mixed and precipitated as metal tungstates. The pH of the solution was adjusted to 8.5 using NaOH. The precipitate was kept in ice-cooled water for 4–5 h, then it was filtered and thoroughly washed with water to make them free from ions. The precipitate was dried at 150°C, homogenized well in an agate mortar and calcinated at 500°C for 5 h in muffle furnace.

2.3. Characterization of photocatalyst

FT-IR analysis was performed using Jasco FT-IR 460 plus spectrophotometer. UV–vis diffuse reflectance spectra (UV-DRS) were recorded on Shimadzu UV-2450 Spectrophotometer equipped with an integrated sphere assembly and $BaSO_4$ used as a reflectance sample. X-ray diffraction (XRD) measurement was carried out to study the crystallographic properties with Bruker AXS Model D8 Advance System using the Cu Kα radiation. The surface area of the photocatalyst was analysed by Micromeritics ASAP 2020 surface area analyser. The surface morphology was studied by AFM image which was taken using Park system AFM XE 100 and field emission scanning electron microscope (FESEM), Carl Zeiss SIGMA with the resolution of 1.2 nm with acceleration voltage of 5 kV. A carbon plate was used for the sampling to avoid charging of the surface. The elements present in the catalyst were investigated using energy dispersive X-ray spectra (EDX) recorded on INCAx-act Oxford Instruments.

2.4. Experimental set-up and photocatalysis procedure

The photocatalytic activity of $CoWO_4$ was studied by decolourization of MO in water using solar, visible and UV light irradiation. The photo reactor for UV light irradiation is immersion well type which consists of two parts. One is quartz tube to place the low pressure mercury pen-ray lamp (provided by cole-parmer) with a maximum emission of about 245 nm. Another one is unsealed borosilicate glass vessel with outer surface water condensation facilities to cancel the heat generated during the photoreaction. The photoreaction under solar light was carried out under bright sunlight between 12 and 2 pm. For visible light irradiation "Heber Visible Annular Type Photo reactor" (as shown in Fig. 1) was used. The photo reactor comprising of a borosilicate immersion jacketed tube to hold the lamp with inlet and outlet for water circulation to cool the lamp. The immersion well is held at the centre of a reaction chamber. The inner surface of reaction chamber is fitted with highly polished anodized aluminium reflector. A 300 W Tungsten Halogen lamp was used for visible light irradiation.

The photocatalytic activity of the sample was evaluated by taking MO at the concentration of 10 ppm and 0.1 g/L of the catalyst at pH 3 otherwise stated. At the given time interval 3.5 mL of the sample was withdrawn and centrifuged to separate the photocatalyst for analysis. The degradation of MO was determined by measuring the maximum absorbance of the sample on UV–visible Spectrophotometer.

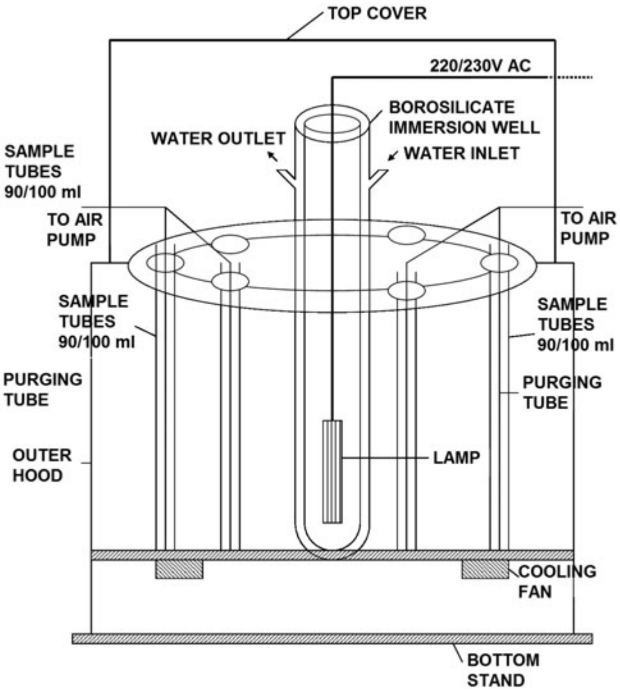

Fig. 1. Schematic diagram of the photocatalytic reactor.

3. Results and discussion

3.1. Characterization of the photocatalyst

3.1.1. X-ray diffraction (XRD)

The crystalline and phase structure of the photocatalyst calcinated at 500˚C was investigated by recording X-ray powder diffraction and shown in Fig. 2. The dhkl and 2θ values of the XRD pattern are well matched with the reported data by ICDD data card [JCPDS no.72–0479]. Metal tungstate, $CoWO_4$ is the wolframite type structure, in which oxygen atoms are in hexagonal closed pack arrangement and Co^{2+} and W^{6+} cations are filled in octahedral sites [20–23]. The average size of the crystal was estimated by Scherrer formula [24] (given in Eq. 1) based on the broadening of (0 0 2) peak at $2\theta = 37^\circ$.

$$D = \frac{K\lambda}{\beta \cos\theta} \tag{1}$$

where D is the crystalline size, K is constant equal to 0.9, λ is wavelength of the radiation used (1.5406 Å), β is the FWHM (full width half maximum) in radians on the 2θ and θ is Bragg angle for the diffraction peak. Based on the Eq. (1), we calculated the crystalline size of the photocatalyst which is to be 17 nm.

3.1.2. FT-IR analysis

The FT-IR spectrum of the prepared photocatalyst is shown in Fig. 3. The mixed metal oxide absorption bands in the FT-IR can be obtained in the region of

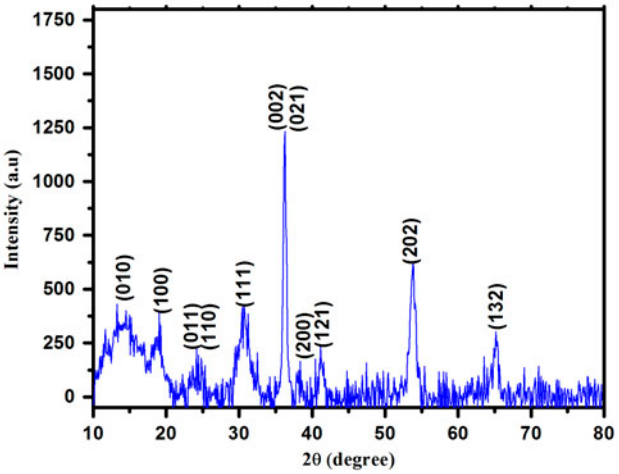

Fig. 2. XRD pattern of $CoWO_4$.

900–400 cm^{-1}, this region corresponds to metal oxygen bond stretching vibration. The absorption band around 890 cm^{-1} assigned to the WO_4 tetrahedron W–O stretching mode [25,26]. The Co-O stretching band was observed around 800 cm^{-1}. The absorption band below 600 cm^{-1} attributed to the deformation of W–O or W–O–W bridges [27].

3.1.3. UV-DRS studies

The optical properties of the prepared catalyst can be obtained by the UV–vis spectroscopic studies and the spectra are shown in Fig. 4. The UV–vis spectrum shows broad line which indicates the absorption in whole of the UV–vis region. The broad absorption spectrum attributed to the presence of multiple consecutive energy levels in the photocatalyst [28].

3.1.4. Morphological study and elemental analysis

The surface morphology of the photocatalyst was illustrated by FESEM analysis and shown in Fig. 5(a) which shows the agglomerated particles. This may be due to sintering the catalyst at high temperature and the image shows irregular arrangement of grains with irregular size. The average particle size calculated to be around 26 nm from the FESEM image. The surface morphology and nanosize of the particle was further confirmed by two dimensional and three dimensional AFM images which are shown in Figs. 5(b) and 5(c), respectively. The size of minimum 36 nm to maximum 46 nm particles was observed in AFM image. The three dimensional AFM image in Fig. 5(c) confirms the irregular arrangement of grains. The BET Surface Area of the photocatalyst was estimated to be 55.0527 m/g. The elemental composition present in the photocatalyst was investigated by recording EDX spectrum that was shown in Fig. 6. The EDX analysis confirms the presence of elements Co, W and O in the photocatalyst.

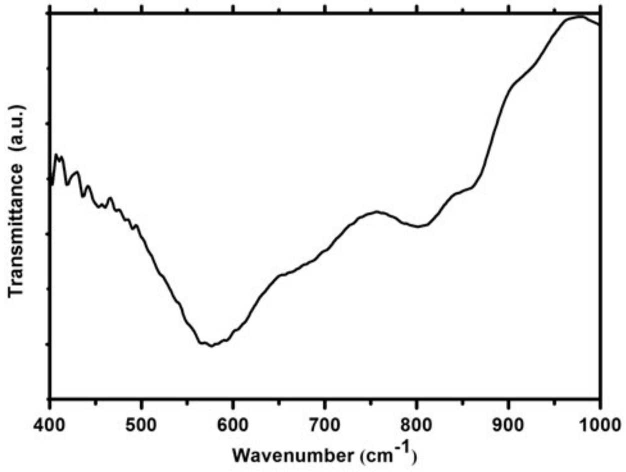

Fig. 3. FT-IR spectrum of $CoWO_4$.

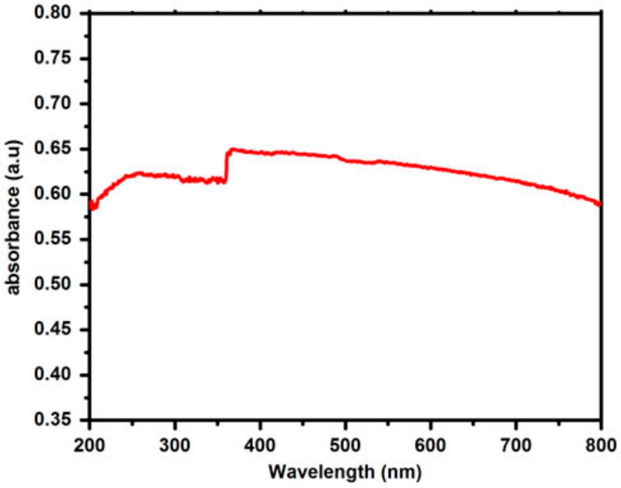

Fig. 4. UV-DRS spectrum of $CoWO_4$.

3.2. Photocatalytic activity

Photocatalytic activity of $CoWO_4$ was investigated by choosing MO as a model pollutant. Fig. 7 shows the time dependent absorption spectrum of the decolourization of MO under solar light. The time dependent absorption spectrum of the decolourization of MO under visible light and UV light at pH 3 is shown in Appendix 1 and 2. Due to the stable intermediate formed on the surface of the photocatalyst, the whole photons cannot be reached to the surface of the photocatalyst, which leads to decrease the rate of decolourization after 10 min. The absorption maximum at 506 nm is due to azo group present in the dye which decreases on increasing irradiation time. At natural pH the absorption maximum of MO will be 463 nm but the maximum absorption is shifted to 506 nm at pH 3. The high photocatalytic activity of $CoWO_4$ under visible light irradiation was achieved when compared with commercially available TiO_2 and shown in Fig. 8. The blank experiment under visible light irradiation shows no significant decolourization. The experimental data reveal that, only adsorption and desorption occurred by TiO_2. High adsorption of 30% was achieved in 20 min then desorbed to 9% in 30 min.

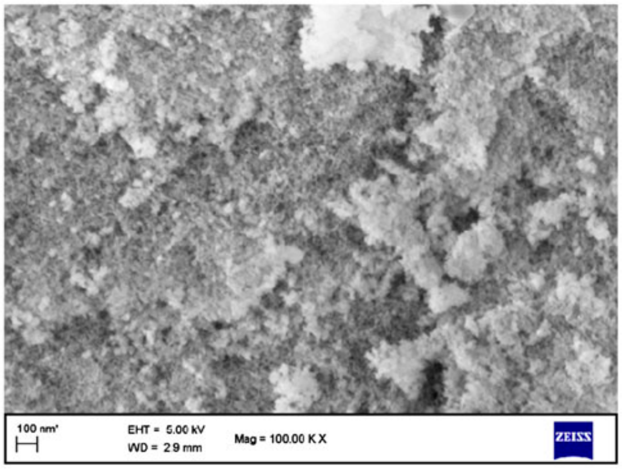

Fig. 5a. FESEM image of $CoWO_4$.

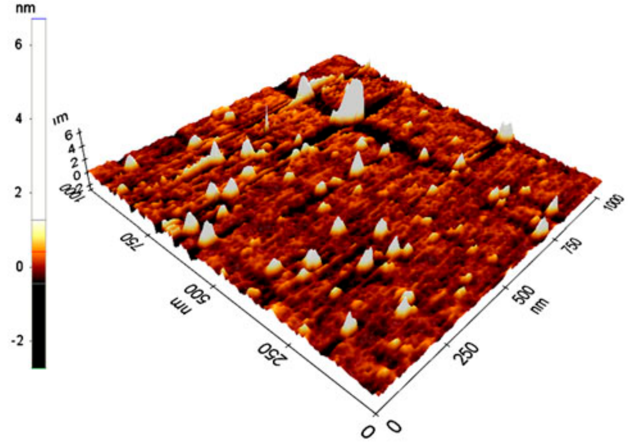

Fig. 5c. Three dimensional AFM image of $CoWO_4$.

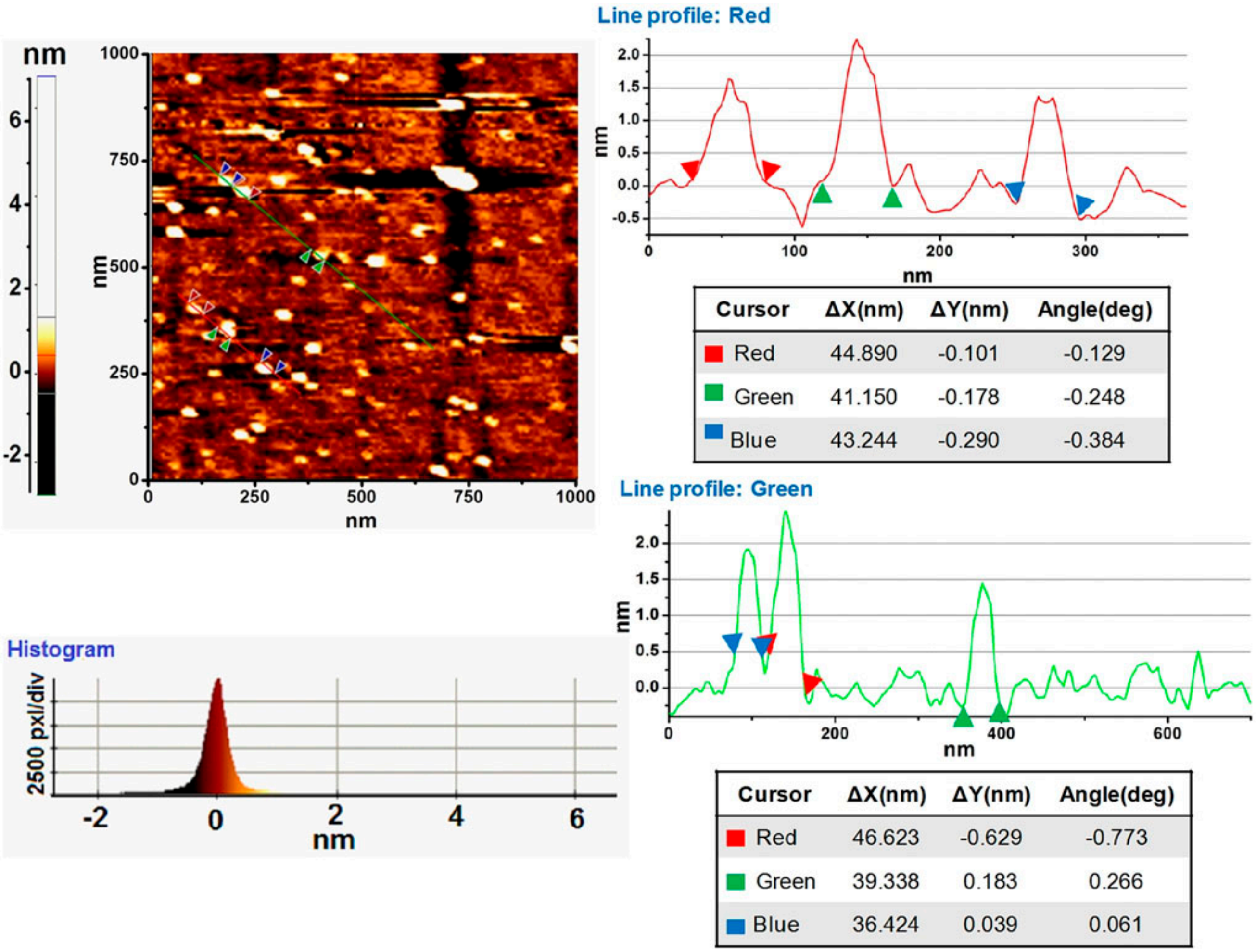

Line profile: Red

Cursor	ΔX(nm)	ΔY(nm)	Angle(deg)
🟥 Red	44.890	-0.101	-0.129
🟩 Green	41.150	-0.178	-0.248
🟦 Blue	43.244	-0.290	-0.384

Line profile: Green

Cursor	ΔX(nm)	ΔY(nm)	Angle(deg)
🟥 Red	46.623	-0.629	-0.773
🟩 Green	39.338	0.183	0.266
🟦 Blue	36.424	0.039	0.061

Fig. 5b. Two dimensional AFM image of $CoWO_4$.

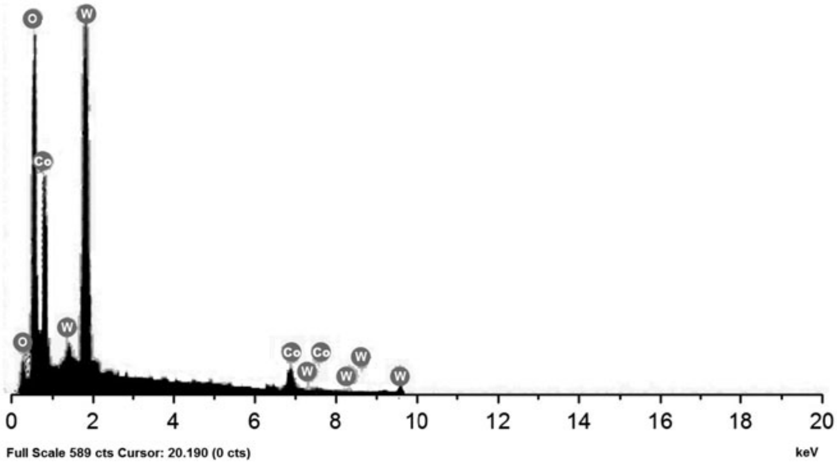

Fig. 6. EDX spectrum of $CoWO_4$.

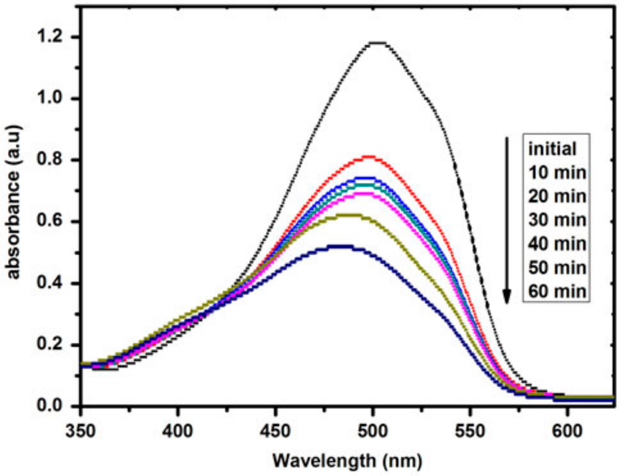

Fig. 7. Time dependent absorption spectrum for the degradation of MO under solar light.

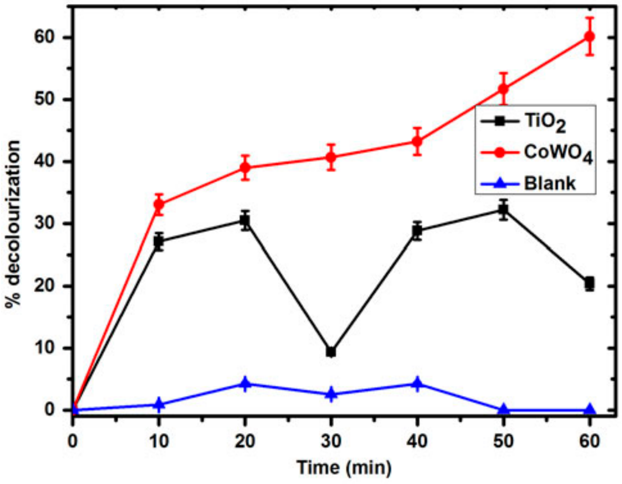

Fig. 8. % Decolourization of MO under Visible light irradiation.

3.2.1. *Effect of light irradiation*

To clarify the photocatalytic efficiency with the effect of different light irradiation, a set of experiments were carried out by changing light irradiation as solar, visible and UV which is shown in Fig. 9 and Appendix 3. The experiment under dark was also conducted to study the role of light on photocatalytic activity. The high photocatalytic efficiency was observed under UV light irradiation which may be due to the high energy of photons. The photocatalytic efficiency of the $CoWO_4$ under solar and visible light irradiation was almost same. Under dark, 51% of the dye molecule has adsorbed in 20 min then desorption was occurred slowly and reached to 18% in 60 min. This experiment under dark suggested that the photocatalyst can be utilized as a good adsorbent for the removal of organic pollutants.

3.2.2. *Effect of catalyst amount*

The amount of catalyst plays a key role on the photocatalytic activity for the decolourization of MO. We investigated the effect of catalyst amount varying from 0.1 g/L to 0.5 g/L at 10 ppm of dye under visible light irradiation and the results are shown in Fig. 10 and Appendix 3. It shows on increasing the amount of catalyst, the efficiency on decolourization of MO increases from 60.17 to 86.44% in 60 min. However, there are no significant changes observed without catalyst under visible light which attributed to the role of

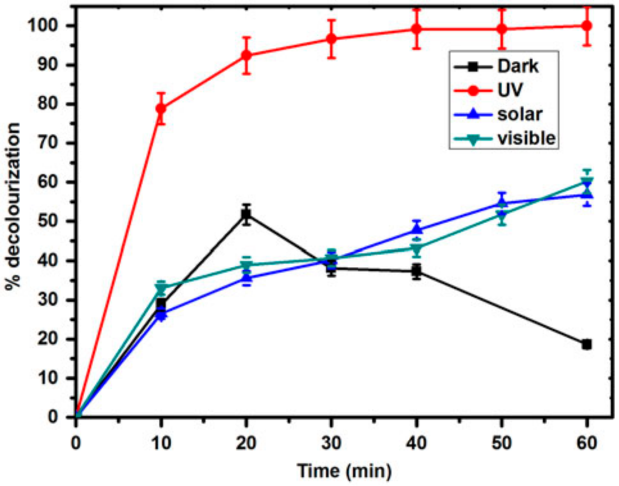

Fig. 9. % Decolourization of MO under different light irradiation.

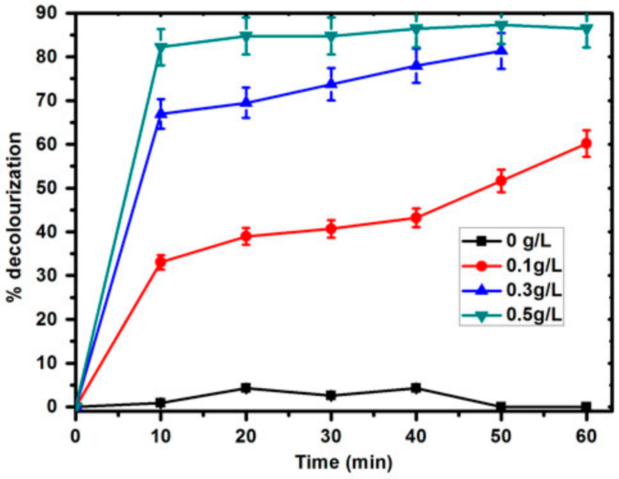

Fig. 10. % Decolourization of MO on varying catalyst amount.

photocatalyst on decolourization of MO. On increasing the catalyst amount, the available active sites increased on the surface of the catalyst at which MO can be adsorbed. More the catalyst amount can enhance the absorption of photons which leads to the high photocatalytic activity.

3.2.3. *Effect of dye concentration*

The effect of various initial dye concentrations from 5 ppm to 20 ppm on the photocatalytic decolourization was studied by keeping 0.1 g/L of catalyst as constant. As shown in Fig. 11 and Appendix 5, the photocatalytic efficiency under visible light irradiation decreases on increasing MO concentration. The active sites of the photocatalyst will be covered by dye molecules as the concentration of MO increases, hence the photons cannot be reached at the surface of the photocatalyst [29,30]. The high concentration of MO will absorb much light required in the photocatalysis thus the decolourization efficiency will decreases [30].

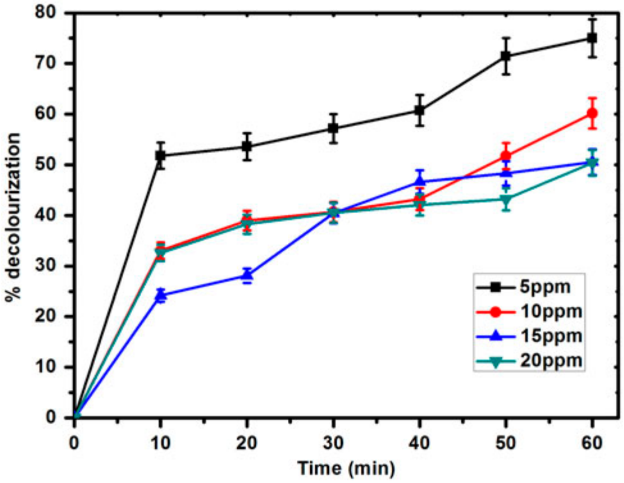

Fig. 11. % Decolourization of MO on varying initial dye concentration.

3.2.4. *Effect of pH*

The effluent from the industry may be in different pH. Therefore, it is important to study the decolorization of MO at various pH. We have demonstrated the decolourization of MO at pH 3, 5, 7 and 9 with 10 ppm of dye concentration under UV light irradiation which shown in Fig. 12 and Appendix 6. The decolourization of MO under other light irradiation was not observed at pH 5, 7 and 9 by $CoWO_4$. The high photocatalytic efficiency at pH 3 of 6.200×10^{-2} and very low efficiency at pH 5 of 2.444×10^{-2} was observed which is shown in Fig. 12. Then, by increasing the initial pH of the solution the photocatalytic activity also increases slightly may be due to the following reason. MO is an anionic dye, at acidic pH the surface of the photocatalyst will be positively charged therefore, adsorption of MO increases as a result the photocatalytic activity increases. The higher pH value can provide high concentration of hydroxyl ions to react with holes to form hydroxyl radicals [31]. At the pH 5, the hydroxyl radical may be present in low concentration and also like charges of photocatalyst and dye molecule may repel each other, this results in the lower efficiency of decolourization. On increasing the pH from 5 to 7 and

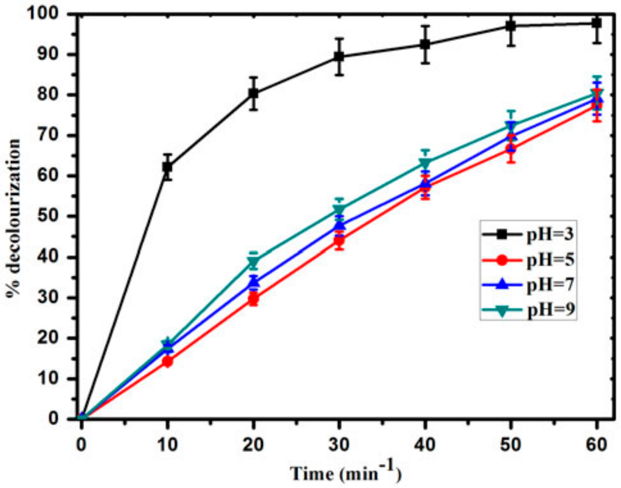

Fig. 12. Effect of pH for the decolourization of MO.

9, due to the presence of hydroxyl ions in high concentration the photocatalytic activity also increases slightly from 2.444×10^{-2} to 2.557×10^{-2} and 2.704×10^{-2} at pH 5, 7 and 9, respectively. The photocatalytic decolourization of MO other than UV irradiation at pH more than 3 was not observed this may be due to the reasons as follows: (1) The like charges of catalyst and dye molecules may repel each other this result in low adsorption of dye on the surface of the photocatalyst (2) lower energy of solar and visible light than that of UV light.

3.3. Kinetic study

The Langmuir–Hinshelwood kinetic equation is more suitable for photocatalytic degradation of many organic dye compounds [32,33]. This can be expressed in Eq. 2 as follows.

$$r = \frac{dC}{dt} = \frac{kKC}{(1 + KC)} \tag{2}$$

In the above equation, KC is very smaller than 1. Integrating the Eq. 2 after neglecting KC with respect to time t, the Eq. 2 can be simplified to a pseudo-first-order kinetic equation (Eq. 3). This equation is represented as follows.

$$\ln\left(\frac{C_o}{C}\right) = kKt = k_{\text{app}}t \tag{3}$$

where r is the rate of the reaction (mol L^{-1} min^{-1}), C_o is the initial concentration of the dye solution (mol L^{-1}), C is the concentration of the dye solution at time t (mol L^{-1}), k is the rate constant (min^{-1}) and K is the adsorption coefficient of the dye on the photocatalyst (L mol^{-1}).

The photocatalytic decolourization of MO follows pseudo-first-order kinetics model. Fig. 13 shows the linear plot of ln (C_o/C) vs irradiation time under different light irradiation and the rate constant of the reaction is given in Table 1. The high rate of about 0.09806 min^{-1} was observed for the decolourization of MO under UV light irradiation. The kinetics profile for the decolourization of MO at different parameters such as amount of catalyst, concentration of dye and initial pH is shown in Figs. 14(a)–(c), respectively, and the rate constant are given in Table 1. As shown in kinetic profile, the rate constant increases on increasing the amount of catalyst. The rate constant decreases on increasing the concentration of dye. On varying the initial pH under UV light irradiation, rate constant is high at pH 3 and decreases to very low at pH 5. Then the rate constant increases on increasing the pH after 5.

3.4. Reaction mechanism

The various photocatalytic process involved in the decolourization of MO is proposed as follows. Upon irradiation, the catalyst will absorb energy in the form of photons which may provide energy to excite the electrons to the bottom of the conduction band and leaving holes in the top of the valence band.

$$CoWO_4 + h\nu \rightarrow e^- + h^+ \tag{4}$$

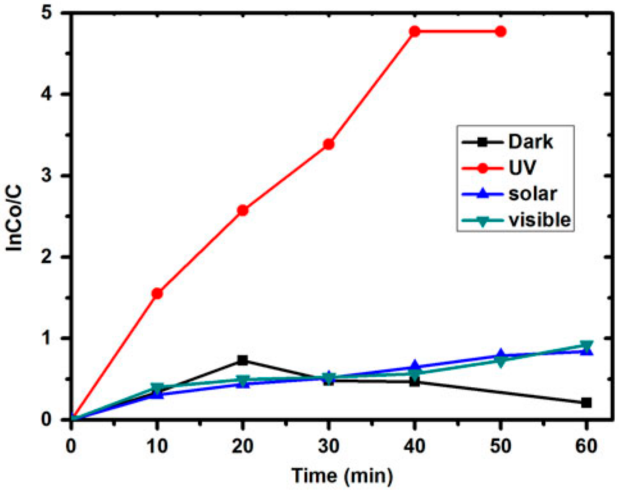

Fig. 13. Kinetic profile for the decolourization of MO under different light irradiation.

Table 1
Rate constant for the decolourization of MO under different light irradiation and at different parameters

On varying light irradiation		Effect of dye concentration		Effect of catalyst amount		Effect of pH	
Light	Rate constant × 10^{-2} (min^{-1})	Dye concentration (ppm)	Rate constant × 10^{-2} (min^{-1})	Catalyst amount (g/L)	Rate constant (min^{-1})	pH	Rate constant × 10^{-2} (min^{-1})
UV	9.806	5	1.919	0	0	3	6.200
Solar	1.317	10	1.245	0.1	0.01245	5	2.444
Visible	1.245	15	1.135	0.3	0.0279	7	2.557
Dark	0.179	20	0.0896	0.5	0.02423	9	2.704

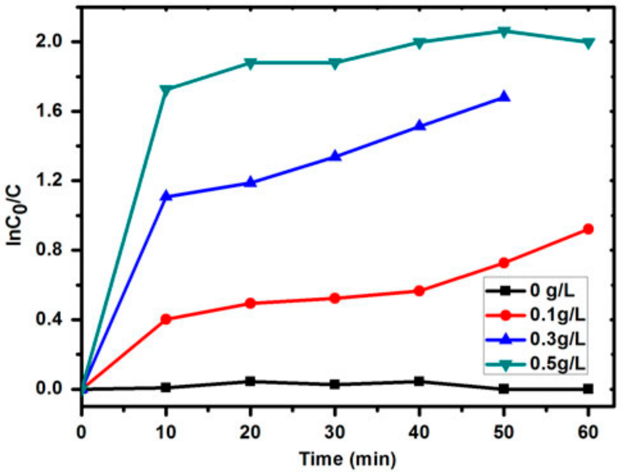

Fig. 14a. Kinetic profile for the decolourization of MO on varying catalyst amount.

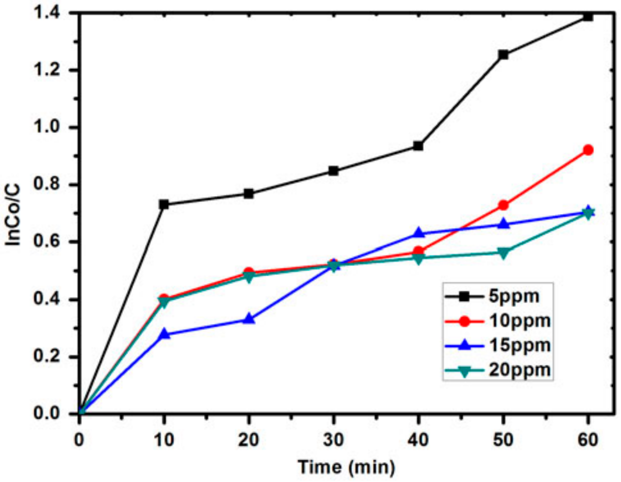

Fig. 14b. Kinetic profile for the decolourization of MO on varying dye concentration.

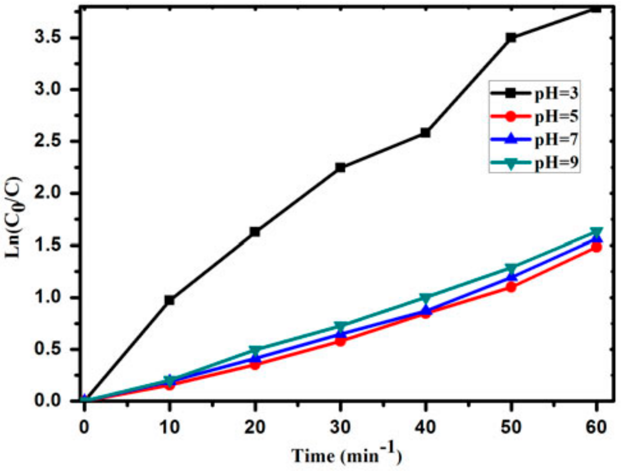

Fig. 14c. Kinetic profile for the decolourization of MO on varying initial pH.

The photogenerated electron-hole pair will migrate to the surface of the catalyst and react with the adsorbed species on the surface.

$$O_2 + 2e^- + 2H^+ \rightarrow H_2O_2 \tag{5}$$

$$H_2O + h^+ \rightarrow \cdot OH + H^+ \tag{6}$$

The active hydroxyl radicals and peroxide formed from the above steps will react with the dye molecule and thus the degradation will occur.

$$\cdot OH/H_2O_2 + MO \rightarrow \text{Products} \tag{7}$$

The photocatalytic decolourization of MO was monitored by UV–vis spectrophotometer in the range of 350–700 nm (visible region). On irradiation of MO with catalyst, the main characteristic band of azo group (–N=N–) in visible region was decreases gradually as shown in Fig. 7. This decrease in the UV–vis spectrum attributed to the degradation of azo group (–N=N–) which results in decolourization of MO.

4. Conclusion

The photocatalyst $CoWO_4$ was successfully synthesized and well characterized by FT-IR, UV-DRS, XRD, EDX, BET, AFM and FESEM techniques. $CoWO_4$ exhibited good photocatalytic activity for the decolourization of MO under different light irradiation (such as solar, visible and UV) at pH 3. The results show minimum amount of (0.1 g/L) catalyst can be effectively decolourize 10 ppm of MO. The enhanced photocatalytic activity was observed under UV light. Moreover, the experiment under dark reveals that the catalyst can be used as a good adsorbent. High surface area of the photocatalyst enhanced the adsorption of anionic dye MO on the surface of the positively charged catalyst at pH 3 hence the activity increased. However, the photocatalytic activity is low at pH 5, this may be due to the presence of hydroxyl radical in low concentration and also like charges of photocatalyst and dye molecule may repel each other. The activity at pH 7 and 9 increases considerably because of the increasing hydroxyl ion concentration at basic pH. We also evaluated the rate constant of the reaction using collected data with the help of Langmuir–Hinshelwood pseudo-first-order kinetics model.

Acknowledgement

The authors thank to DST-SERC for financial support, sanction no. SR\FT\CS-042\2008 and Anna University, BIT Campus, (erstwhile Anna University of Technology Tiruchirappalli) Tiruchirappalli, for supporting to carry out this work.

References

[1] K.L. Sajjad, S. Shamaila, B. Tian, F. Chen, J. Zhang, Comparative studies of operational parameters of degradation of azo dyes in visible light by highly efficient WO_x/TiO_2 photocatalyst, J. Hazard. Mater. 177 (2010) 781–791.

[2] K. Rajeshwar, M.E. Osugi, W. Chanmanee, C.R. Chenthamarakshan, M.V.B. Zanoni, P. Kajitvichyanukul, R. Krishnan-Ayer, Heterogeneous photocatalytic treatment of organic dyes in air and aqueous media, J. Photochem. Photobiol. C: Photochem. Rev. 9 (2008) 171–192.

[3] A. Fujishima, K. Honda, Electrochemical photolysis of water at a semiconductor electrode, Nature 238 (1972) 37–38.

[4] M.H. Habibi, R. Kamrani, Photocatalytic mineralization of methylene blue from water by a heterogeneous copper-titania nanocomposite film, Desalin. Water Treat. 46 (2012) 278–284.

[5] H.L. Wang, D.Y. Zhao, W.F. Jiang, VIS-light-induced photocatalytic degradation of methylene blue (MB) dye using PoPD/TiO_2 composite photocatalysts, Desalin. Water Treat. 51 (2013) 2826–2835.

[6] S.C. Zhang, J.D. Shen, H.B. Fu, W.Y. Dong, Z.J. Zheng, L.Y. Shi, Bi_2WO_6 photocatalytic films fabricated by layer-by-layer technique from Bi_2WO_6 nanoplates and its spectral selectivity, J. Solid State Chem. 180 (2007) 1456–1463.

[7] A.P. Finlayson, V.N. Tsaneva, L. Lyons, M. Clark, B.A. Glowacki, Evaluation of Bi-W-oxides for visible light photocatalysis, Phys. Status Solidi A 203 (2006) 327–335.

[8] S.C. Zhang, J.D. Shen, H.B. Fu, W.Y. Dong, Z.J. Zheng, L.Y. Shi, Bi_2WO_6 photocatalytic films fabricated by layer-by-layer technique from Bi_2WO_6 nanoplates and its spectral selectivity, J. Solid State Chem. 180 (2007) 1456–1463.

[9] J. Mo, Y. Zhang, Q. Xu, J.J. Lamson, R. Zhao, Photocatalytic purification of volatile organic compounds in indoor air: A literature review, Atmos. Environ. 43 (2009) 2229–2246.

[10] Y. Cong, J.L. Zhang, F. Chen, M. Anpo, Synthesis and characterization of nitrogen-doped TiO_2 nanophotocatalyst with high visible light activity, J. Phys. Chem. C 111 (2007) 6976–6982.

[11] W.K. Ho, J.C. Yu, S. Lee, Synthesis of hierarchical nanoporous F-doped TiO_2 spheres with visible light photocatalytic activity, Chem. Commun. 10 (2006) 1115–1117.

[12] R. Asahi, T. Morikawa, T. Ohwaki, K. Aoki, Y. Taga, Visible-light photocatalysis in nitrogen-doped titanium oxides, Science 293 (2001) 269–271.

[13] H. Irie, Y. Watanabe, K. Hashimoto, Nitrogen-concentration dependence on photocatalytic activity of $TiO_{2-x}N_x$ powders, J. Phys. Chem. B 107 (2003) 5483–5486.

[14] H. Fu, C. Pan, L. Zhang, Y. Zhu, Synthesis, characterization and photocatalytic properties of nanosized Bi_2WO_6, $PbWO_4$, and $ZnWO_4$ catalysts, Mater. Res. Bull. 42 (2007) 696–706.

[15] S.H. Yu, B. Liu, M.S. Mo, J.H. Huang, X.M. Liu, Y.T. Qian, General synthesis of single-crystal tungstate nanorods/nanowires: A facile, low-temperature solution approach, Adv. Funct. Mater. 13 (2003) 639–647.

[16] J. Lin, J. Lin, Y. Zhu, Controlled synthesis of the $ZnWO_4$ nanostructure and effects on the photocatalytic performance, Inorg. Chem. 46 (2007) 8372–8378.

[17] G. Huang, C. Zhang, Y. Zhu, $ZnWO_4$ photocatalyst with high activity for degradation of organic contaminants, J. Alloy. Compd. 432 (2007) 269–276.

[18] G. Huang, Y. Zhu, Enhanced photocatalytic activity of $ZnWO_4$ catalyst via fluorine doping, J. Phys. Chem. C 111 (2007) 11952–11958.

[19] T. Montini, V. Gombac, A. Hameed, L. Felisari, G. Adami, P. Fornasiero, Synthesis, characterization and photocatalytic performance of transition metal tungstates, Chem. Phys. Lett. 498 (2010) 113–119.

[20] D. Chen, Z. Liu, S. Ouyang, J. Ye, Simple room-temperature mineralization method to $SrWO_4$ micro/nanostructures and their photocatalytic properties, J. Phys. Chem. C 115 (2011) 15778–15784.

[21] S.J. Naik, A.V. Salker, Mechanistic approach of CO oxidation over $Cu_{1-x}Co_xWO_4$ system, Catal. Commun. 10 (2009) 884–888.

[22] P.K. Pandey, N.S. Bhave, R.B. Kharat, Spray deposition process of polycrystalline thin films of $CuWO_4$ and study on its photovoltaic electrochemical properties, Mater. Lett. 59 (2005) 3149–3155.

[23] A. Sen, P. Pramanik, A chemical synthetic route for the preparation of fine-grained metal tungstate powders (M=Ca, Co, Ni, Cu, Zn), J. Eur. Ceram. Soc. 21 (2001) 745–750.

[24] L.J. Burcham, I.E. Wachs, Vibrational analysis of the two non-equivalent, tetrahedral tungstate (WO_4) units in $Ce_2(WO_4)_3$ and $La_2(WO_4)_3$, Spectrochim. Acta A 54 (1998) 1355–1368.

[25] T. Mathew, N.M. Batra, S.K. Arora, Electrical conduction in $CuWO_4$ crystals, J. Mater. Sci. 27 (1992) 4003–4008.

[26] M. Galceran, M.C. Pujol, C. Zaldo, F. Díaz, M. Aguiló, Synthesis, structural, and optical properties in monoclinic Er:$KYb(WO_4)_2$ nanocrystals, J. Phys. Chem. C 113 (2009) 15497–15506.

[27] H. Zhang, X. Hu, Catalytic oxidation of carbon monoxide in a fixed bed reactor, Sep. Purif. Technol. 34 (2004) 105–108.

[28] Y. Gao, J. Zhao, Y. Zhu, S. Ma, X. Su, Z. Wang, Wet chemical process of rod-like tungsten nanopowders with iron (II) as reductive agent, Mater. Lett. 60 (2006) 3903–3905.

[29] E. Tomaszewicz, Reactivity in the solid state between $CoWO_4$ and RE_2WO_6 where RE=Sm, Eu, Gd, Thermochim. Acta 447 (2006) 69–74.

[30] G. Li, Y. Zhang, L. Wu, F. Wu, R. Wang, D. Zhang, J. Zhu, H. Li, An efficient round-the-clock La_2NiO_4 catalyst for breaking down phenolic pollutants, RSC Adv. 2 (2012) 4822–4828.

[31] C.S. Lu, Y.T. Wu, F.D. Mai, W.S. Chung, C.W. Wu, W.Y. Lin, C.C. Chen, Degradation efficiencies and mechanisms of the ZnO-mediated photocatalytic degradation of Basic Blue 11 under visible light irradiation, J. Mol. Catal. A: Chem. 310 (2009) 159–165.

[32] M.A. Rauf, S.S. Ashraf, Fundamental principles and application of heterogeneous photocatalytic degradation of dyes in solution, Chem. Eng. J. 151 (2009) 10–18.

[33] M.A. Barakat, H. Schaffer, G. Hayes, S. Ismat-Shah, Photocatalytic degradation of 2-chlorophenol by Co-doped TiO_2 nanoparticles, Appl. Catal. B. 57 (2004) 23–30.

Appendix 1

Time dependent absorption spectrum for the degradation of MO under visible light irradiation at pH=3.

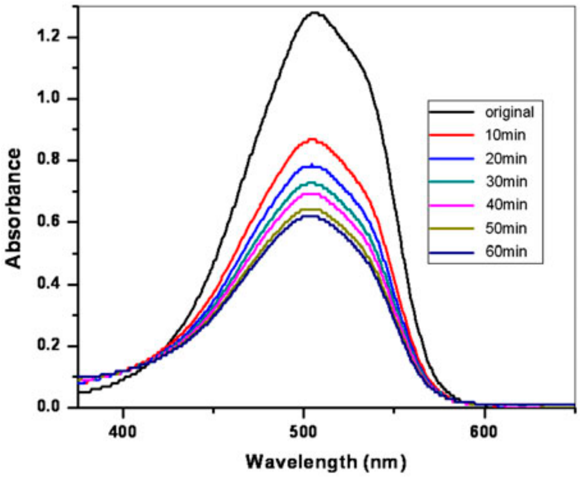

Calculation of %Decolourization:

The % decolourization was calculated using the following formula

$$\%D = \frac{(C^{\circ} - C)}{C} \times 100$$

Where, %D is % decolourization of MO, C_0 is the initial concentration of the MO solution; C is the concentration of MO solution at time t.

Appendix 2

Time dependent absorption spectrum for the degradation of MO by UV light irradiation at pH=3.

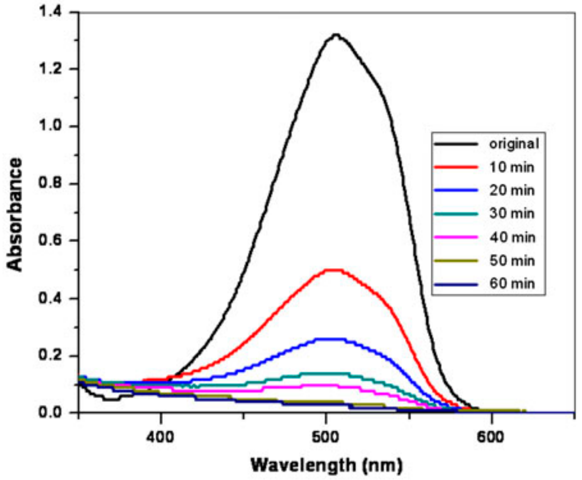

Appendix 3

Plot of C/C_0 as a function of irradiation time under different light irradiation for the decolourization of MO.

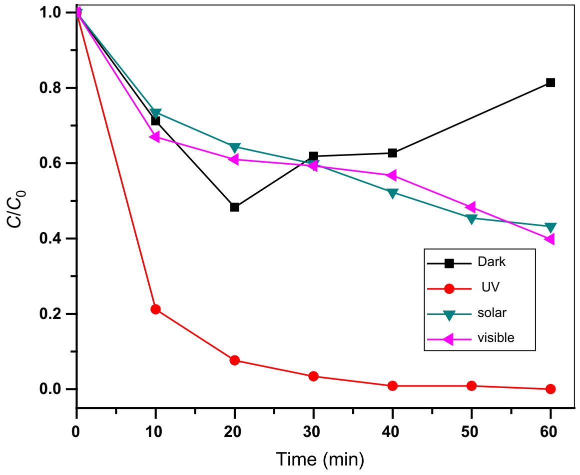

Appendix 4

Plot of C/C_0 as a function of irradiation time for the decolourization of MO on varying catalyst amount.

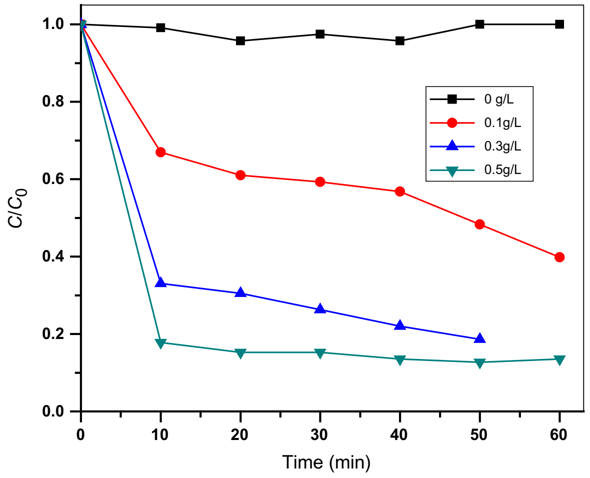

Appendix 5

Plot of C/C_0 as a function of irradiation time for the decolourization of MO on varying dye concentration.

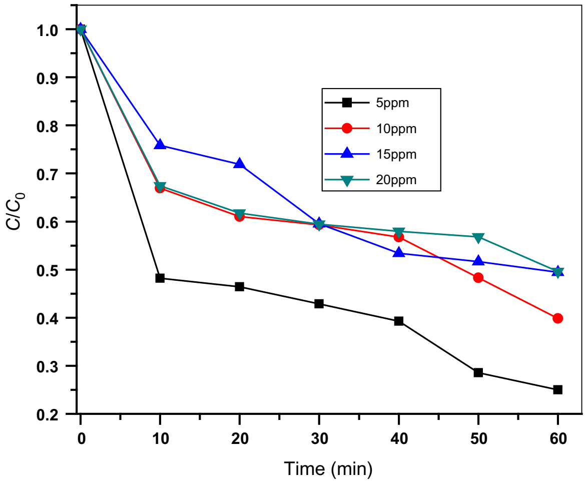

Appendix 6

Plot of C/C_0 as a function of irradiation time at different pH for the decolourization of MO under UV light irradation.